Progress In Electromagnetics Research C, Vol. 149, 187-197, 2024 PIER C

(Received 15 September 2024, Accepted 24 October 2024, Scheduled 8 November 2024)

Compact Dual-Band CPW-Fed Circularly Polarized Slot Antenna for GNSS Applications

Ahmed G. Salama[1,*], Osama M. Dardeer[2], Angie R. Eldamak[1], and Hadia M. El-Henawy[1]

[1]*Electronics and Communications Engineering Department, Faculty of Engineering, Ain Shams University, Cairo 11566, Egypt*
[2]*Microstrip Department, Electronics Research Institute (ERI), El Nozha, Cairo 12622, Egypt*

ABSTRACT: This paper introduces a compact dual-band circularly polarized (CP) slot antenna utilized for L-band Global Navigation Satellite Systems (GNSS) applications. The designed antenna structure is a printed L-shaped slot antenna (PLSA) fed by coplanar waveguide (CPW) with a squared ground plane. An L-shaped feeding line is protruded into an L-shaped slot to achieve a circular polarization operation. A reversed T-stub is adopted near the right center of the radiating patch in order to achieve a dual-band operation. The achieved fractional impedance bandwidths (FIBWs) are 5.6% (1.21–1.28 GHz) and 12.2% (1.46–1.65 GHz). The fractional axial ratio bandwidths (FARBWs) are 8.0% (1.21–1.31 GHz) and 18.0% (1.42–1.70 GHz) for the lower and upper GNSS ranges, respectively. The suggested antenna provides right-hand circular polarization (RHCP) radiation. The gain of the suggested antenna ranges between 3.0 dBic and 3.2 dBic for the lower and upper GNSS bands, respectively. The designed antenna exhibits a dual-band behavior that covers both the lower and upper GNSS bands. It has a low profile of $55 \times 55 \times 1.524\,\text{mm}^3$ $(0.22\lambda_0 \times 0.22\lambda_0 \times 0.006\lambda_0)$, which makes it suitable for incorporating within any portable devices receiving GNSS signals. The antenna is lightweight, small in size, inexpensive with simple structure, high FARBW, high FIBW, and demonstrates CP dual-band behavior with a single input. The antenna is simulated, fabricated, and measured. The measurements verify the numerical results successfully. The suggested antenna is suitable for GNSS applications due to its enhanced performance.

1. INTRODUCTION

In recent years, many different applications have made leverage of global navigation satellite systems (GNSSs). A more accurate navigational solution can be achieved by utilizing multiple systems (especially because there are more observable satellites). Interestingly, each navigation satellite system has a unique modulation form and signal format, which inherently guards against interference caused by frequency overlap. GNSSs comprising a US Global Positioning System (GPS), a Russian GLONASS, a Chinese BeiDou, and a European Galileo. They send their communications in the radio frequency L-band with the left-hand circular polarization (LHCP) technique to ensure reliable communication [1]. As illustrated in Fig. 1, GNSSs operate in a pair of frequency bands (1164–1300 MHz) and (1559–1610 MHz), which have been selected exclusively for the use by radio navigation satellite services (RNSSs). Precise orientation is not necessary for GNSS transmitting and receiving antennas. As a result, GNSSs have made extensive use of circularly polarized (CP) antennas. GNSS satellites use highly directive (high-gain) antennas for transmitting signals, while receiving antennas usually have low gain, enabling a wide angle of reception [2, 3]. Thus, GNSS receiving antennas need to be compact, Right Hand Circularly Polarized (RHCP), lightweight, easily integrable, and operating in dual-band frequency to reject unwanted frequencies.

Various methodologies have been explored to design CP antennas for GNSS applications, including cross-dipole [4, 5], printed helical [6], and microstrip patch antennas [7–21] which have been extensively researched. Fractional impedance bandwidth (FIBW), fractional axial ratio bandwidth (FARBW), half power beamwidth (HPBW), and axial ratio beamwidth (ARBW) are important factors affecting the antenna performance in navigation applications [3]. In addition to these factors, the most important challenge is obtaining miniaturized antennas due to the usage of low frequencies in GNSS standards. Thus, microstrip patch antenna has long been a focal point of GNSS research because of its low profile, cost-effectiveness, simplicity of fabrication, ease of integration, and lightweight properties despite its several major drawbacks, including limited power handling capacity, low gain, and narrow bandwidth [22]. To overcome these drawbacks by designing very small antennas with broad bandwidth and acceptable gain, two different approaches have been utilized in the previous literature, namely, broadband and multiband techniques. Firstly, the broadband technique, such as the antenna in [4], used two printed perpendicular dipoles coupled with four metallic cylinders to broaden the FIBW up to 43% (from 1.08 GHz to 1.69 GHz). In [5], two intersected dipoles fed by a broadband feeding network surrounded by a notched-corner cavity are used to widen the HPBW to 110° while the ARBW is 130° in the operating band. The antenna covers all GNSS frequency ranges with a FIBW of 54.07% (from 1.06 GHz to 1.86 GHz), a FARBW of 48.06% (from 1.08 GHz to 1.78 GHz), and the peak

* Corresponding author: Ahmed G. Salama (2002453@eng.asu.edu.eg).

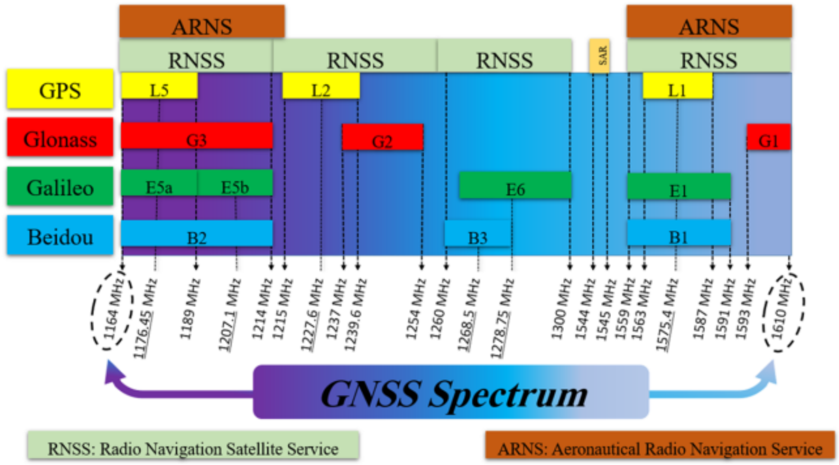

FIGURE 1. Assigned L-band frequencies for navigation satellite applications.

gain is 3.5 dBi. The antenna size is $70 \times 70 \times 30\,\text{mm}^3$ ($0.32\lambda_0 \times 0.32\lambda_0 \times 0.17\lambda_0$). A cone shaped printed helical antenna with an L-shaped strip is designed in [6] to enhance the FIBW and FARBW. The antenna has an Overlapped Fractional Bandwidth (OFBW) of 40.3% (from 1.13 GHz to 1.7 GHz), peak gain of 6.4 dBi, and size is $100 \times 100 \times 3\,\text{mm}^3$ ($1\lambda_0 \times 0.7\lambda_0 \times 0.7\lambda_0$). In [7], loading four arcs on the main radiator is used to expand the ARBW to 232°, 241°, 212°, and 244° at $\varphi = 0°$, 45°, 90°, and 135°, respectively. The antenna covers BeiDou Navigation System B1 with a FIBW of 5.13% (from 1.52 GHz to 1.6 GHz), a FARBW of 1.28% (from 1.55 GHz to 1.57 GHz), and the maximum gain is 4.09 dBi. The antenna size is $100 \times 100 \times 3\,\text{mm}^3$ ($0.52\lambda_0 \times 0.52\lambda_0 \times 0.0156\lambda_0$). In [8], there are four parasitic branches that resemble claws at each corner of the ground to expand the HPBW to 116° overall CP bandwidth, the FIBW to 72.5%, and the FARBW to 54%, simultaneously. The antenna size is $0.35\lambda_0 \times 0.35\lambda_0 \times 0.06\lambda_0$, and the maximum gain is 3.4 dBi. In [9], a cylindrical sandwiched structure that includes a circular disc with center capacitive feeding is used to widen the HPBW to 132° overall CP bandwidth and to expand FIBW and FARBW to 32.5% and 37.6%, respectively. The antenna size is $0.34\lambda_0 \times 0.34\lambda_0 \times 0.05\lambda_0$, and the peak gain is 2.1 dBic. However, broadband antennas are found suffering from a bulky profile and receiving unwanted frequencies.

Secondly, the multi-band technique, such as the antenna in [10], which uses incorporated shorting probes, allows the antenna to operate at two bands. In order to generate two or more resonance frequencies and cover a wider IBW, stacked patches are used in [11, 12], and hexagonal shape fractal iterations are employed in [13]. Additionally, by using mechanical or electrical switches, different IBWs can be reached by a frequency-reconfigurable antenna [14]. In [15], dual-band CP operation at GPS L2 and L5 bands with a miniaturized size has been accomplished by etching a pair of asymmetric spiral slots into the radiator. The antenna size is $59.64 \times 59.64 \times 1.6\,\text{mm}^3$ ($0.24\lambda_0 \times 0.24\lambda_0 \times 0.006\lambda_0$). It has FIBWs of (2.54%, 3.97%), FARBWs of (0.76%, 0.73%), and peak gains of (4 dBi, 3.52 dBi) for L2 and L5 GPS bands, respectively. In [16], the FIBWs are enhanced to 9.4% (from 1.164 GHz to 1.279 GHz) and 2.3% (from 1.579 GHz to 1.616 GHz) using a right/left hand hybrid transmission line to balance the phase difference between the four feeding ports in the feed network. The antenna size is $70 \times 70 \times 19.5\,\text{mm}^3$ ($0.29\lambda_0 \times 0.29\lambda_0 \times 0.08\lambda_0$), and it achieves a maximum gain of 4.9 dBic. A significant size reduction of 54% has been reported by using a multilayer pentagon ring antenna in [17]. The antenna size is $50 \times 50 \times 3.2\,\text{mm}^3$ ($0.21\lambda_0 \times 0.21\lambda_0 \times 0.013\lambda_0$). It has FIBWs of (1.7%, 1.8%), FARBWs of (1.0%, 1.3%), and peak gains of (2.52 dBi, 3.35 dBi), for L5 and L1 GPS frequency bands, respectively. Multilayer hexagonal antennas have been used in [18, 19] to cover GPS frequency bands (L1, L2, and L5). In [19], the FIBWs are increased to 2.7% (from 1.163 GHz to 1.195 GHz) and 2.1% (from 1.561 GHz to 1.595 GHz), FARBWs enhanced to 2.3% (from 1.167 GHz to 1.195 GHz) and 2.0% (from 1.558 GHz to 1.590 GHz), and peak gains raised to 3.41 dBi and 3.62 dBi for L5 and L1 GPS frequency bands, respectively. The antenna size is $55 \times 55 \times 3.2\,\text{mm}^3$ ($0.22\lambda_0 \times 0.22\lambda_0 \times 0.013\lambda_0$). These antennas [17–19] have been developed from an equilateral triangular patch antenna, which can operate at lower frequencies with a smaller patch size than the square and circular microstrip antennas. In [20], only a single patch with a single feed has been presented by adding four distinct structured slots to the radiator. The suggested antenna adds another feature that enables reconfigurable RHCP for GPS and LHCP for Satellite Digital Audio Radio Service (SDARS) applications, respectively. The antenna size is $65 \times 65 \times 1.6\,\text{mm}^3$. The antenna in [21] demonstrates a dual-band CP design that covers the lower and upper (GNSS) bands by using a metallic cavity containing two antennas inspired by metasurfaces. The first one offered a creative way to produce dual-band behavior with dimensions of $60 \times 60 \times 20\,\text{mm}^3$ ($0.23\lambda_0 \times 0.23\lambda_0 \times 0.08\lambda_0$ at the frequency of 1164 MHz). The second one is to achieve CP behavior using two feeds connected to the radiating patch with dimensions of $50 \times 50 \times 20\,\text{mm}^3$ ($0.26\lambda_0 \times 0.26\lambda_0 \times 0.11\lambda_0$ at the frequency of 1559 MHz). The antenna peak gain is 3.2 dBi over the GNSS frequency range. Through research in previous literature, it was found that the antenna's large size, narrow FIBW,

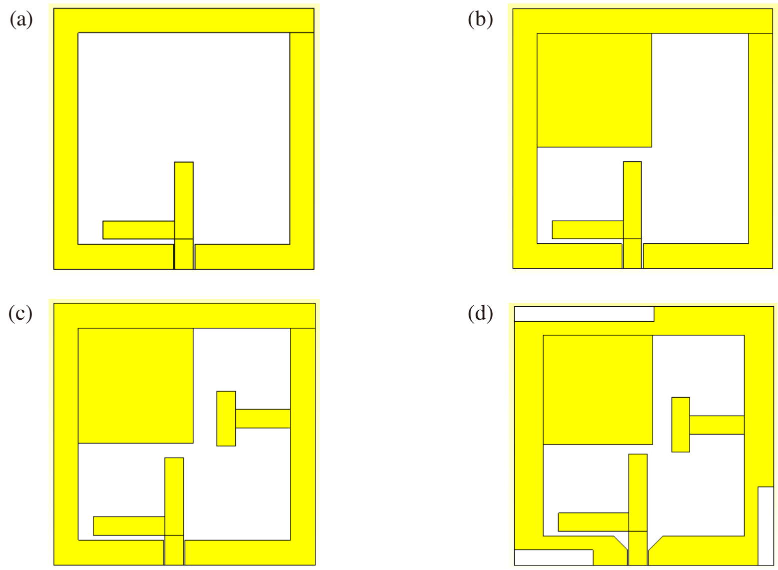

FIGURE 2. Evolutionary stages of the designed antenna: (a) Antenna-a, (b) Antenna-b, (c) Antenna-c, (d) Antenna-d.

narrow FARBW, and complicated feeding structures make it less portable.

This paper proposes a compact dual-band CP aperture antenna for modern GNSS applications operating in the L-band. This antenna achieves a wide FARBW and broadened FIBW while remaining compact in comparison to the previous designs, whereas the suggested antenna covers both the lower and upper GNSS bands (L1, L2, B1, B2, G1, G2, E1) with miniaturized dimensions of $55 \times 55 \times 1.524\,\text{mm}^3$ $(0.22\lambda_0 \times 0.22\lambda_0 \times 0.006\lambda_0)$. It has a wide FARBW of 8.0% (1.21–1.31 GHz) and 18.0% (1.42–1.70 GHz). It has a broadened FIBW of 5.6% (1.21–1.28 GHz) and 12.2% (1.46–1.65 GHz) for the lower and upper GNSS ranges, respectively. This paper uses a slot antennas as its basis. A slot antenna is characterized by its wide bandwidth with small size due to the electrically long structure in a small area. Thus, the idea of this paper was based on using a squared slot antenna to increase the effective slot length to be able to decrease the overall antenna size while achieving the needed bandwidth [23]. In order to excite a pair of near-degenerate orthogonal modes that cause CP behavior, an L-shaped feeding line has been protruded into an asymmetrical L-shaped slot [24, 25]. An inverted-T stub has been adopted near the middle-right edge of the slot to achieve a dual-band operation. The suggested design comprises a printed L-shaped slot with an embedded inverted-T stub excited by an L-shaped microstrip feeding line. It was fed by a coplanar waveguide (CPW) with a squared ground plane. The suggested antenna accomplished all GNSS needs: RHCP radiation, dual-band operation, high FARBW, high FIBW, wide beamwidth, high radiation efficiency, compact size, light weight, cost effectiveness, and a flatness gain. High correlations are found between the measured and simulated results. The arrangement of the paper is as follows. The design and realization procedures for the squared slot antenna are explained in Section 2. Parametric analyses are given in Section 3. Results and measurement processes are illustrated in Section 4. Evaluation and comparison with recent designs of GNSS antennas are detailed in Section 5. The paper is concluded in Section 6.

2. ANTENNA DESIGN AND REALIZATION STEPS

Figure 2 displays the four design stages that went into the antenna creation.

2.1. Squared Slot Antenna with L-Shaped Feedline (Antenna-a)

The squared slot antenna is designed on the top of a single substrate layer that consists of a high-performance material (Rogers RO4003c). The substrate measures a thickness (h) of 1.542 mm with a dielectric constant (ε_r) of 3.55 and a low tangential loss tan(δ) of 0.0027. As observed in Fig. 2(a), the initial stage of the antenna design process involves creating a square slot with dimensions of $W_s \times L_s$. The square slot dimensions can be estimated from the resonance frequency at $f_r = 1.37\,\text{GHz}$, as follows [26]:

$$f_r = \frac{c}{2(L_s+W_s)\sqrt{\varepsilon_{reff}}} \tag{1}$$

where ε_{reff} is the effective dielectric constant represented by:

$$\varepsilon_{reff} = \frac{\varepsilon_r+1}{2} + \frac{\varepsilon_r-1}{2}\left(1+\frac{12h}{W}\right)^{-1/2} \tag{2}$$

where ε_r is the substrate relative permittivity; c the light speed in the free space; L_s and W_s are the slot length and width, respectively. The typical antenna overall dimensions were determined to be marginally larger than W_s, as follows:

$$L = W > W_s \tag{3}$$

where L and W stand for the antenna overall length and width, respectively, as shown in Fig. 2(a). The squared slot antenna is fed by a 50-ohm CPW feeding technique with an L-shaped microstrip feedline at the same layer and two g-wide gaps (between feed line and ground plane). The microstrip feedline ends with an L-shaped tuning stub with dimensions (l_1, l_2) for length and w_f for width. By correctly adjusting l_1 and l_2, the CP behavior is produced by exciting a pair of near-degenerate orthogonal modes. The feedline is positioned as indicated in Fig. 2(a) near the middle of the antenna, w_2 away from the left edge of the radiating slot. Using the CST studio suite, a squared slot antenna with an L-shaped feedline is simulated.

2.2. Square Slot with Embedded Corner Stub and L-Shaped Feedline (Antenna-b)

To achieve a good circular polarization, the slot with an asymmetrical shape is essential due to its nonuniform shape [27, 28]. It has a phase difference between its electric field components, which produces a circular polarization. Asymmetry is introduced into the slot shape by adding a square stub to the squared slot upper-left corner, as seen in Fig. 2(b), to improve the CP performance. The squared stub can be derived by multiplying the slot by the scaling factor (SF). The squared stub has length l_a and width w_a, which are specified as follows:

$$l_a = SF \times L_s \tag{4}$$

$$w_a = SF \times W_s \tag{5}$$

Antenna-b is simulated with various SF values. Fig. 3 displays the reflection coefficient $|S_{11}|$ of the antenna-b at SF equal to 0.50, 0.525, 0.55, and 0.575. SF is set to 0.55, which satisfies the needed reflection coefficient $|S_{11}|$ with the resonance frequency at $f_r = 1.37$ GHz. The incorporation of a squared stub to form an L-shaped slot significantly improved both of IBW and ARBW for antenna-b, as shown in Figs. 5 and 6. By optimizing placement of the L-shaped tuning stub at the end of the feeding line, the impedance matching and IBW have been enhanced. Thus, the L-shaped feeding line is shifted in the direction of the left ground surface edge as shown in Fig. 2(b) to improve the impedance matching and IBW by increasing the coupling between the radiating slot and microstrip feeding line.

2.3. L-Shaped Slot with Embedded Inverted-T Stub and L-Shaped Feedline (Antenna-c)

To cover the upper and lower GNSS frequency ranges, two operational resonant frequencies are adjusted by loading an inverted-T stub close to the middle right edge of the L-shaped slot as shown in Fig. 2(c). The introduction of the first resonance frequency f_{r1} is attributed to the L-shaped slot [29], while the second resonance frequency f_{r2} is caused by adopting an inverted-T stub. This w_f-wide inverted-T stub has horizontal and vertical lengths (t_1, t_2) and a d-distance apart from the slot's lower border. It behaves as a perturbed element that modifies the stored magnetic and electric elements due to the coupling between the resonators [30] based on the principle of shape perturbation theory, since the operating frequencies vary according to the electric, magnetic, and total energies stored in the cavity.

2.4. L-Shaped Slot with Embedded Inverted-T Stub and Corner Cropped Slits Fed by L-Shaped Feedline (Antenna-d)

To enhance the ARBW of the proposed antenna, three corner cropped slits with optimized dimensions are engraved in the bottom-left, bottom-right, and upper-left corners of the squared slot aperture as shown in Fig. 2(d) [31]. Also, two chamfered edges are etched at the ground on both sides of the feed line [32]. Fig. 6 shows that antenna-d ARBW is expanded and overlapped with impedance bandwidth due to the etched cropped slits. The suggested dual-band antenna layout is displayed in Fig. 4. The design parameters of the designed antenna are optimized using CST Microwave Studio (CST MWS). Optimized dimensions of the antenna are displayed in Table 1. The impacts of each design iteration from antenna-a to antenna-d on $|S_{11}|$ and axial ratio are illustrated in Figs. 5 and 6, respectively.

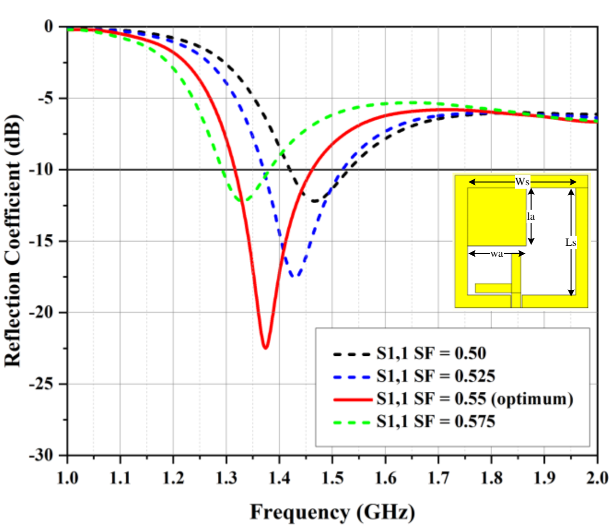

FIGURE 3. Simulated reflection coefficient $|S_{11}|$ of the antenna-b at distinct values of SF.

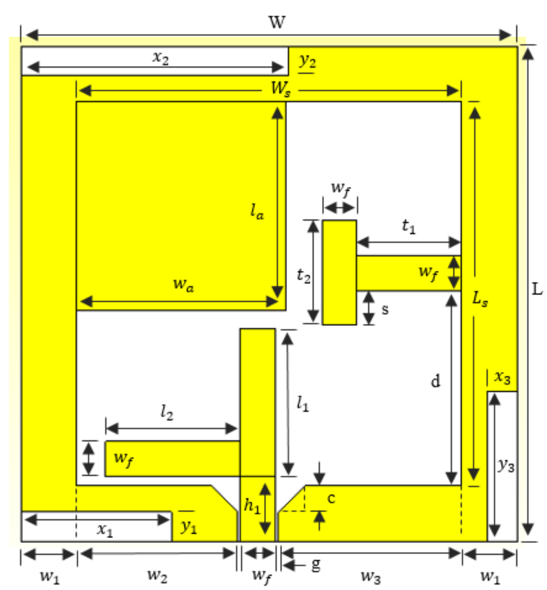

FIGURE 4. Geometry of the designed antenna at the top view.

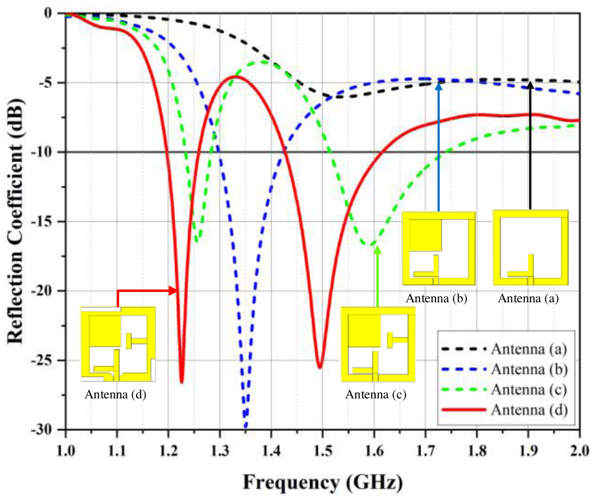

FIGURE 5. Simulated reflection coefficient $|S_{11}|$ at the design steps.

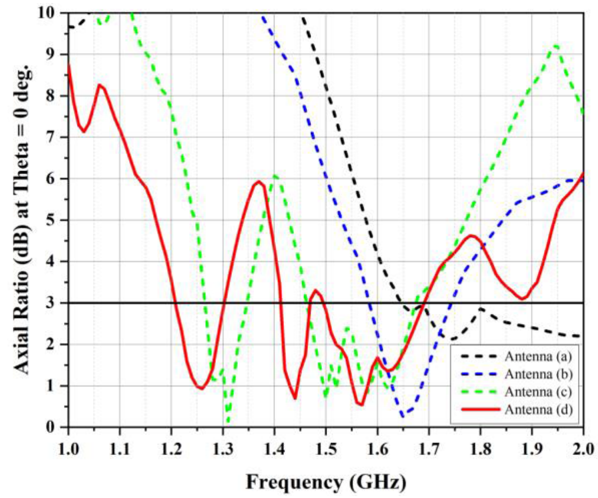

FIGURE 6. Simulated axial ratio at the design steps at Theta $= 0°$.

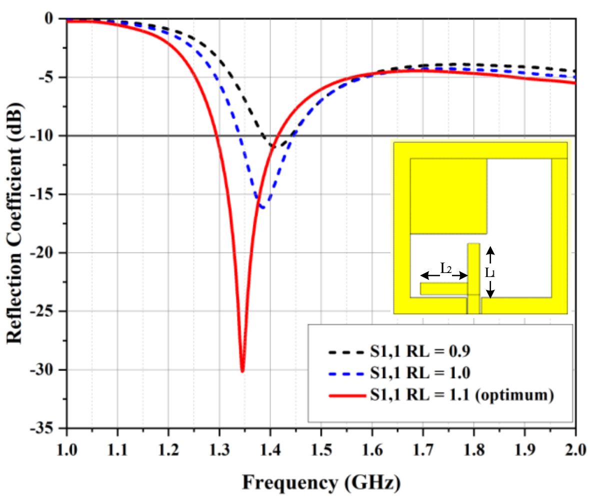

FIGURE 7. Simulated reflection coefficient $|S_{11}|$ of the antenna-b at distinct values of R_L.

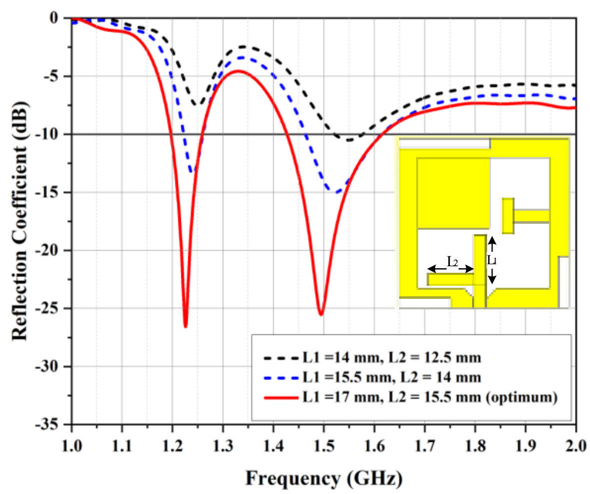

FIGURE 8. The impact of l_1 and l_2 on the impedance bandwidth.

TABLE 1. The optimized dimensions of the designed antenna.

Symbol	Value (mm)	Symbol	Value (mm)
L	55	l_1	17
W	55	l_2	15.5
h	1.524	t_1	12
l_s	44	t_2	12
W_s	44	d	22.5
w_f	4	s	4
h_1	6.7	x_1	17.5
g	0.35	y_1	3.5
w_1	5.6	x_2	31
w_2	17.3	y_2	3.5
w_3	21.8	x_3	3.5
l_a	24	y_3	17.5
w_a	24	c	2.7

3. PARAMETRIC ANALYSES

Utilizing CST Microwave Studio, parametric studies were performed. The impact of different parameters on the axial ratio (AR) bandwidth and reflection coefficient $|S_{11}|$ is explained by a variety of simulation results. This section modifies one parameter only, with the remaining parameters unchanged.

3.1. Step 1: Studying the Effect of the Lengths of the Vertical and Horizontal L-Shaped Feedline Arms (l_1, l_2)

First, we examine an antenna (antenna-b) that is not connected to a grounded inverted-T stub and get the optimum R_L to achieve the required center frequency at $f_r = 1.37\,\text{GHz}$. R_L is the ratio between the horizontal and vertical arm lengths of the L-shaped feeding line, as follows:

$$R_L = l_1/l_2 \tag{6}$$

While the other parameters remain constant, antenna-b is simulated at various values of R_L, as shown in Fig. 7.

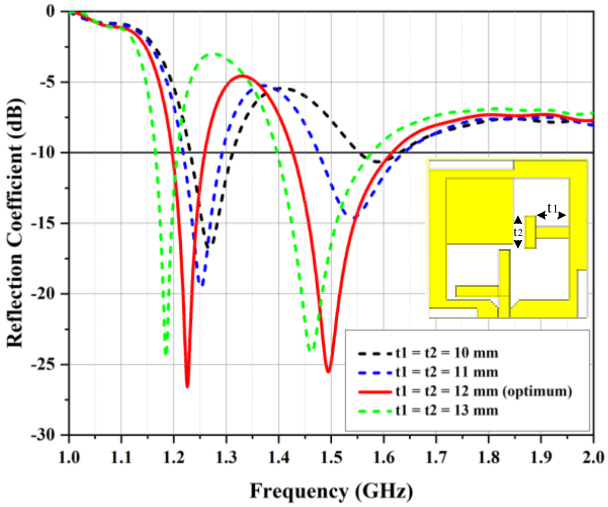

FIGURE 9. The impact of t_1 and t_2 on the impedance bandwidth.

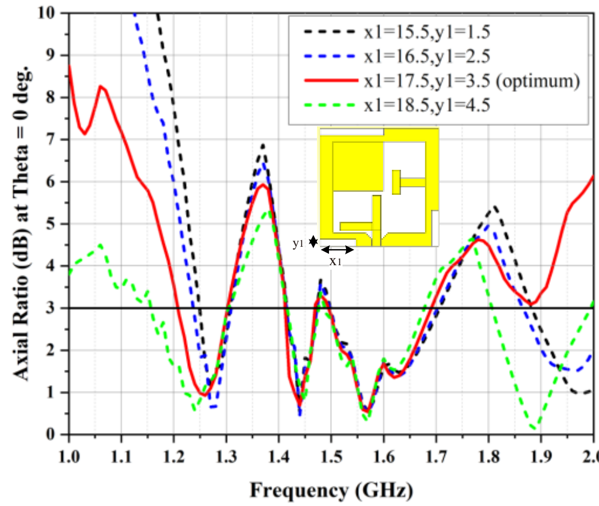

FIGURE 10. The impact of the slit-1 dimensions x_1 and y_1 on the axial ratio bandwidth at Theta $= 0°$.

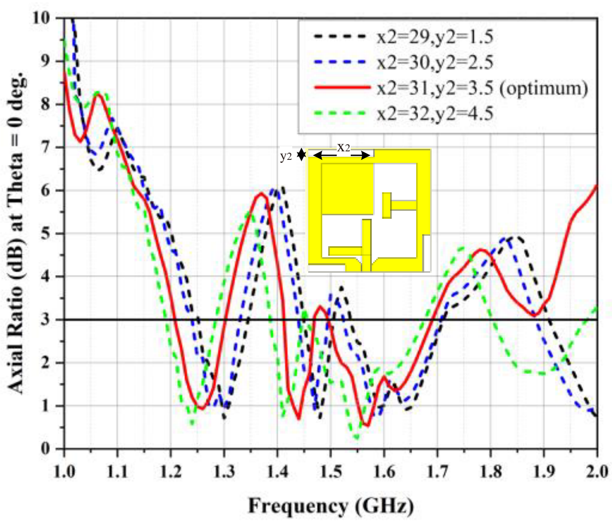

FIGURE 11. The impact of the slit-2 dimensions x_2 and y_2 on the axial ratio bandwidth at Theta $= 0°$.

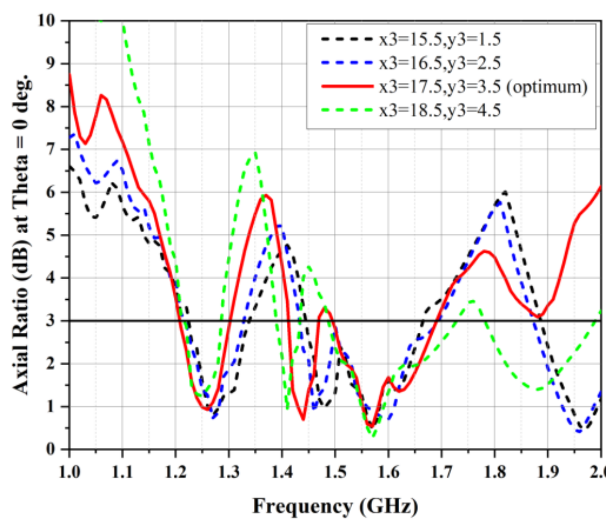

FIGURE 12. The impact of the slit-3 dimensions x_3 and y_3 on the axial ratio bandwidth at Theta $= 0°$.

It is found that the optimal CP frequencies can be obtained as long as $R_L \simeq 1.1$ because both l_1 and l_2 are limited to being integral multiples of a half-millimeter [33]. Then, we apply a parametric study on the lengths of L-shaped feedline arms (l_1, l_2). The designed antenna is simulated at various values of (l_1, l_2), while the other parameters remain constant. Fig. 8 illustrates how the simulated IBW is varied according to the lengths of the vertical and horizontal L-shaped feedline arms (l_1, l_2). As the lengths l_1 and l_2 increase, the simulated IBW is widened, the starting frequency shifted downwards, and the impedance matching increased.

3.2. Step 2: Studying the Effect of the Lengths of the Vertical and Horizontal Inverted-T Stub Arms (t_1, t_2)

Figure 9 shows how varying the length t_1, t_2 affects the simulated $|S_{11}|$. The results of the simulation indicate that the operating frequencies are shifted downward, and the impedance matching is increased as t_1, t_2 is increased. It is interesting that changing the parameter t_1, t_2 allows for easy control of the antenna resonant frequency position in the operating bands and enhances the impedance matching.

3.3. Step 3: Studying the Effect of the Lengths of the Vertical and Horizontal Corner Cropped Slits (x_n, y_n)

Figures 10, 11, 12 illustrate that the ARBW is varied according to the slit dimensions (x_n, y_n). As shown in Fig. 10, when the slit-1 dimensions (x_1, y_1) increase, the ARBW is slightly shifted downwards to the required frequency band and slightly increased in the lower frequency band. Also, as shown in Figs. 11 and 12, when slit-2 and slit-3 dimensions (x_2, y_2) and (x_3, y_3) increase, the ARBW is slightly shifted downwards to the required frequency band.

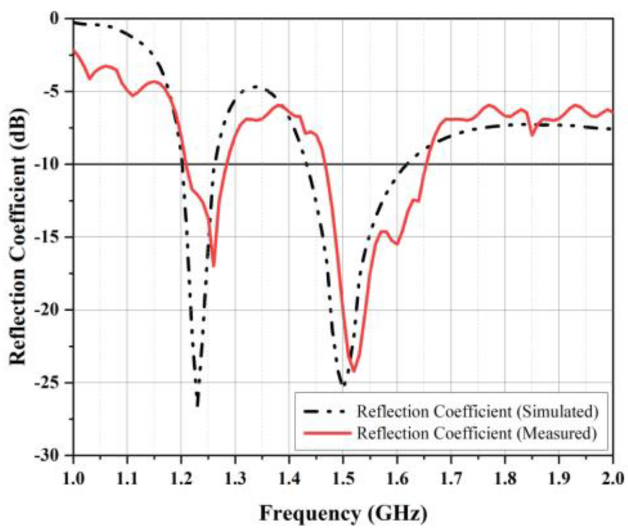

FIGURE 13. $|S_{11}|$ measured and simulated results.

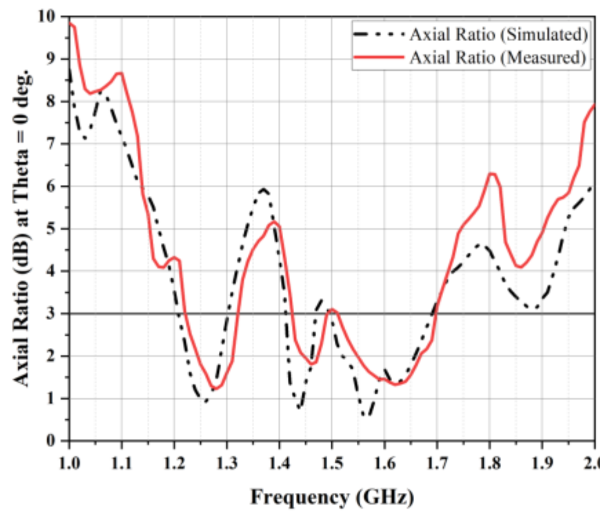

FIGURE 14. 3-dB AR simulated and measured results at Theta $= 0°$.

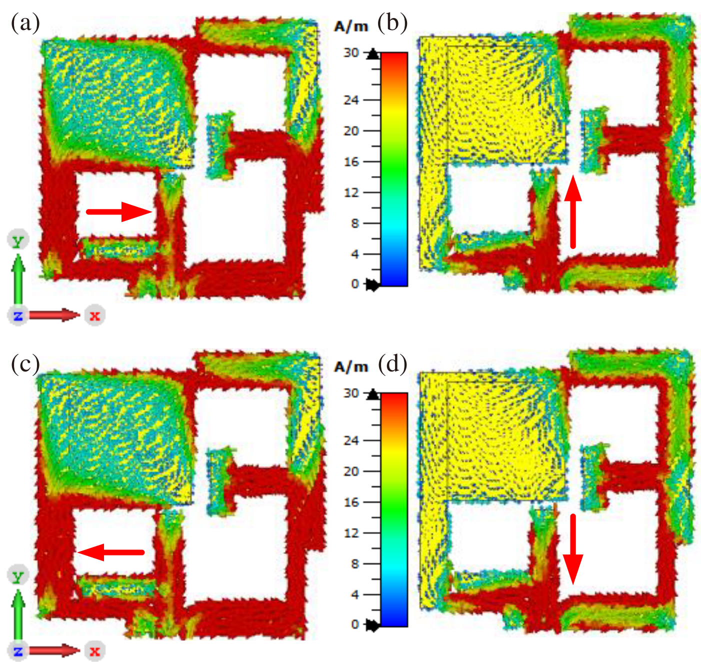

FIGURE 15. Current distribution of the suggested antenna at 1.5 GHz at angels of: (a) 0°, (b) 90°, (c) 180°, (d) 270°.

4. RESULTS AND MEASUREMENTS

This section illustrates the simulated and measured results for the designed antenna parameters and radiation patterns. The fabricated antenna prototype is also presented along with its measurement procedures. The fabricated suggested antenna undergoes testing for validation. Utilizing an Agilent E8363B Vector Network Analyzer (VNA), the antenna reflection coefficient $|S_{11}|$ is measured. The antenna's far field is assessed using the SATIMO system. The most GNSS frequency bands are covered by both the simulated and measured results. The antenna's measured and simulated reflection coefficients $|S_{11}|$ are depicted in Fig. 13. The measured -10 dB bandwidths are 70 MHz (5.6% FIBW) expanding from 1210 MHz to 1280 MHz and 190 MHz (12.2% FIBW) expanding from 1460 MHz to 1650 MHz, whereas the simulated -10 dB bandwidths predict a 65 MHz (5.3% FIBW) expanding from 1200 MHz to 1265 MHz and 170 MHz (11.2% FIBW) expanding from 1440 MHz to 1610 MHz. The measured results of $|S_{11}|$ agree closely with the simulated ones.

In Fig. 14, measured and simulated axial ratios (ARs) demonstrate that the antenna is circularly polarized in the wanted frequency bands. The measured 3-dB AR bandwidths are 100 MHz (8.0% FARBW) expanding from 1210 MHz to 1310 MHz and 280 MHz (18.0% FARBW) expanding from 1420 MHz to 1700 MHz, whereas the simulated AR 3-dB bandwidths predict a 100 MHz (8.0% FARBW) expanding

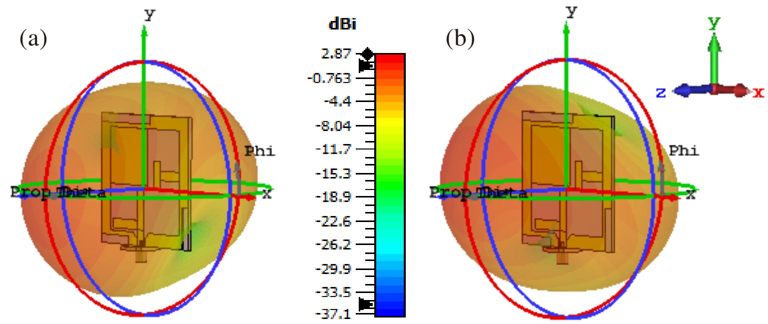

FIGURE 16. 3D radiations of the suggested antenna at distinct frequencies: (a) 1.25 GHz, (b) 1.5 GHz.

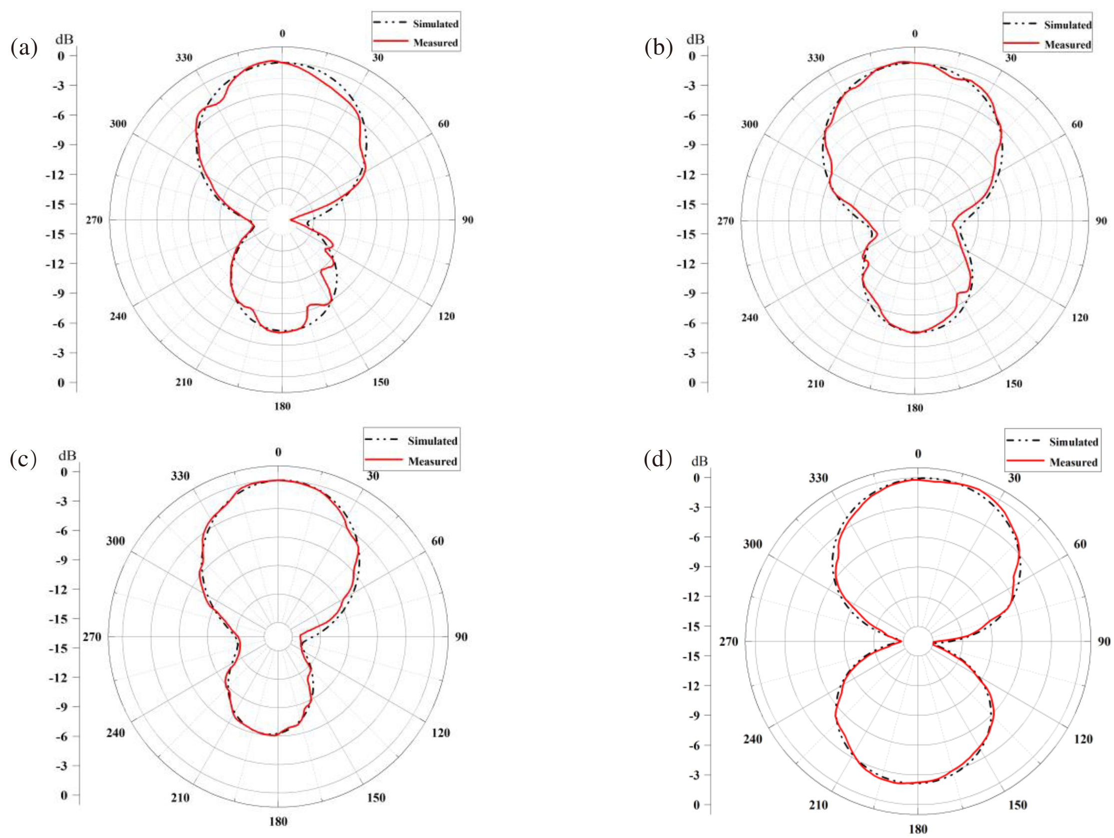

FIGURE 17. The simulated and measured normalized field patterns of the suggested antenna at: (a) E-plane at $f = 1.25$ GHz, (b) H plane at $f = 1.25$ GHz, (c) E-plane at $f = 1.5$ GHz,(d) H-plane at $f = 1.5$ GHz.

from 1200 MHz to 1300 MHz and 280 MHz (18.0% FARBW) expanding from 1410 MHz to 1690 MHz. There is a strong agreement between the measured AR and the corresponding simulation results.

The surface current that was simulated at 1.5 GHz in Fig. 15 demonstrates the circular polarization property mechanism. The surface current distribution is a critical parameter determining the antenna radiation characteristics. Figs. 15(a), 15(b), 15(c), and 15(d) display the surface current distributions at four different phase angles of 0, 90, 180, and 270 degrees. It can be seen from comparing each phase with its predecessor that the surface current rotates anticlockwise with a 90° increment in the phase angle. As a result, right-hand circularly polarized radiation (RHCP) is produced in the positive z direction (antenna front).

Figure 16 displays the 3D radiations of the suggested antenna elements at distinct frequencies (1.25, 1.5 GHz).

A SATIMO anechoic chamber is utilized to measure the antenna radiation pattern. Figs. 17(a), 17(b), 17(c), and 17(d) illustrate the E-plane (phi $= 0°$) and H-plane (phi $= 90°$) radiation patterns at frequencies of 1.25 GHz and 1.5 GHz for simulated and manufactured antennas. As a result, the designed antenna radiates in the $+z$ direction at the upper hemisphere (antenna front side) and in the $-z$ direction at the lower hemisphere (antenna back side), due to no copper at the bottom of the substrate. It is obvious that the measured and simulated ra-

TABLE 2. Comparison with other published articles.

Ref.	Size (mm^3)	Frequency (GHz)	No. of GNSS bands covered	Feed	10 dB FIBW (%)	3 dB FARBW(%)	Overlapped FBW (%)	Max Gain (dBic)
[15]	$59.6 \times 59.6 \times 1.6$ $(0.24 \times 0.24 \times 0.006)\lambda_0^3$	1.176 , 1.227	L5, L2	Single coaxial feed	2.54 , 3.97	0.76 , 0.73	0.76 , 0.73	3.52 , 4.0
[16]	$70 \times 70 \times 19.5$ $(0.29 \times 0.29 \times 0.08)\lambda_0^3$	1.221 , 1.597	L2,L5, B2,B3, E5, G1,G2,G3	4-way power divider	9.4 , 2.3	NA	1.0 , 1.3	4.9 , 4.9
[17]	$5 \times 5 \times 3.2$ $(0.21 \times 0.21 \times 0.013)\lambda_0^3$	1.176 , 1.575	L1, L5	Single coaxial feed	1.7 , 1.8	1.0 , 1.3	1.0 , 1.3	2.52 , 3.35
[18]	$86 \times 86 \times 3.2$ $(0.34 \times 0.34 \times 0.013)\lambda_0^3$	1.176 , 1.575	L1, L5	Single coaxial feed	2.5 , 2.7	1.5 , 1.0	1.5 , 1.0	3.68 , 3.31
[20]	$65 \times 65 \times 1.6$ $(0.26 \times 0.26 \times 0.006)\lambda_0^3$	1.176 , 2.332	L5	Single coaxial feed	4.0 , 4.2	1.1 , 1.0	1.1 , 1.0	4.2 , 6.6
[21]	$50 \times 50 \times 20$ $(0.26 \times 0.26 \times 0.11)\lambda_0^3$	1.575	L1, B1, E1	Two coaxial probes	414	952	414	3.2
[19]	$55 \times 55 \times 3.2$ $(0.22 \times 0.22 \times 0.013)\lambda_0^3$	1.176 , 1.575	L1, L5	Single coaxial feed	2.7 , 2.1	2.3 , 2.0	2.3 , 2.0	3.41 , 3.62
This work	$55 \times 55 \times 1.524$ $(0.22 \times 0.22 \times 0.006)\lambda_0^3$	1.245 , 1.555	L1,L2, B1,B2, E1, G1,G2	CPW	5.6 , 12.2	8.0 , 18.0	5.62 , 12.2	3.0 , 3.2

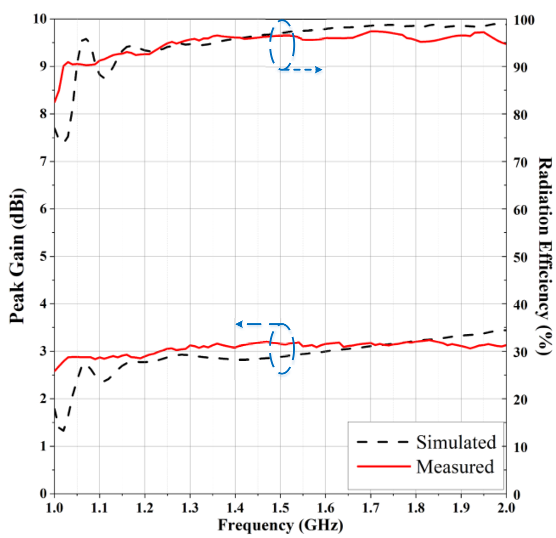

FIGURE 18. Measured and simulated results for both antenna radiation efficiency and gain.

diation patterns are strongly correlated. The antenna operates well throughout the most GNSS frequency bands, according to the radiation pattern result.

The measured and simulated antenna radiation efficiencies and maximum gains across the full range of GNSS frequency bands are displayed in Fig. 18. The suggested antenna achieves a maximum measured radiation efficiency of 96% and a maximum measured gain of 3.2 dBic. Fabrication tolerances are the primary reason of the slight variation between the measured and simulated efficiencies. The suggested antenna maximum peak gain is slightly lower than those found in [6–21], since there is no reflective element on the back of the suggested antenna.

The front view of the manufactured squared slot antenna is photographed in Fig. 19. The antenna parameters were measured for the manufactured antenna using an Agilent E8363B Vector Network Analyzer (VNA) and a SATIMO anechoic chamber as shown in Figs. 20(a) and 20(b), respectively.

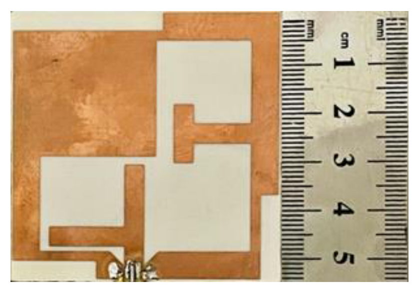

FIGURE 19. The suggested antenna prototype.

5. EVALUATION AND COMPARISON

This section provides a detailed comparison between the suggested slot antenna and a number of modern GNSS antenna designs, as listed in Table 2. A comprehensive evaluation of various antenna designs is given in the table with respect to antenna size, number of the covered GNSS bands, impedance bandwidth, axial ratio (3-dB bandwidth), and maximum gain. The suggested design performs remarkably well in the needed band in terms of bandwidth, compact size, simple structure, and circular polarization. The proposed layout is smaller than majority of the other designs, measuring only $55 \times 55 \times 1.524\,\mathrm{mm}^3$ $(0.22\lambda_0 \times 0.22\lambda_0 \times 0.006\lambda_0)$, which qualifies it for the use in GNSS handheld applications. The overlapped circularly polarized bandwidths of the proposed design are 70 MHz, which covers from 1210 MHz to 1280 MHz and 190 MHz, which cov-

(a) (b)

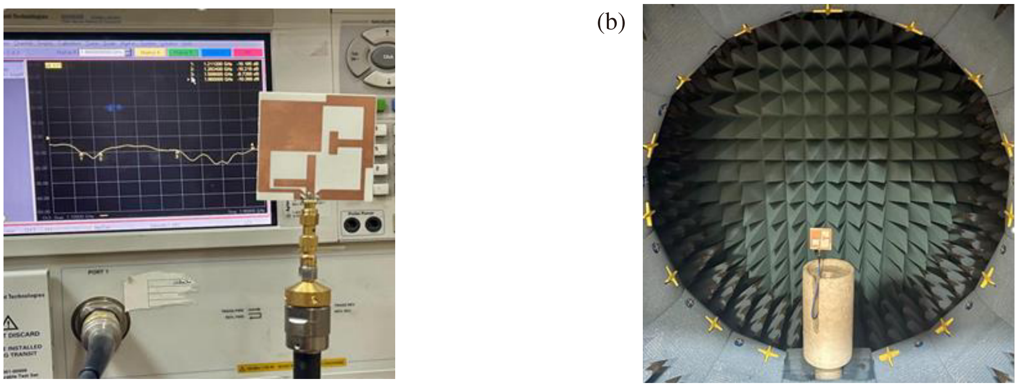

FIGURE 20. Photos taking during the measurements process utilizing: (a) Agilent E8363B vector network analyzer, (b) SATIMO system.

ers from 1460 MHz to 1650 MHz, and are remarkably wide in comparison to the other designs in terms of bandwidth. It covers almost lower and upper GNSS bands (L1, L2, B1, B2, G1, G2, E1) compared to the recent designs. According to this study, the proposed GNSS antenna design offers superior performance over existing designs.

6. CONCLUSION

This paper offers the design, simulation, fabrication, and testing of a dual-band squared slot antenna with an incorporated L-shaped feedline and an inverted-T stub. An introduction and illustrations are provided for the process of obtaining the dual-band operation from a miniaturized square slot antenna and enhancing the axial ratio (AR) and bandwidth. The antenna covers the majority of GNSS frequency bands with dual-band circularly polarized bandwidths of 70 MHz from 1210 MHz to 1280 MHz and 190 MHz from 1460 MHz to 1650 MHz. The achieved 3 dB axial ratio bandwidths are 100 MHz from 1210 MHz to 1310 MHz and 280 MHz from 1420 MHz to 1700 MHz. The antenna achieves RHCP radiation. Antenna gain ranges between 3.0 dBic and 3.2 dBic. The antenna has a light weight and a compact size with dimensions $55 \times 55 \times 1.524\,\text{mm}^3$ $(0.22\lambda_0 \times 0.22\lambda_0 \times 0.006\lambda_0)$, which make it more practical for GNSS handheld applications. The antenna has achieved a high radiation efficiency of 96%. We have evaluated the performance of the proposed antenna design through measurements on a manufactured prototype, and the results show that the design is reliable.

REFERENCES

[1] Gleason, S. and D. Gebre-Egziabher, "GNSS application and methods," *Chem. Biodivers.*, Vol. 1, No. 11, 1829–1841, 2004.

[2] Teunissen, P. J. G. and O. Montenbruck, *Springer Handbook of Global Navigation Satellite Systems*, Springer, 2017.

[3] Wang, J. J. H., "Antennas for global navigation satellite system (GNSS)," *Proceedings of the IEEE*, Vol. 100, No. 7, 2349–2355, 2012.

[4] Hussine, U. U., Y. Huang, and C. Song, "A new circularly polarized antenna for GNSS applications," in *2017 11th European Conference on Antennas and Propagation (EUCAP)*, 1954–1956, Paris, France, Mar. 2017.

[5] Li, C., F.-S. Zhang, F. Zhang, and K. Yang, "A wideband circularly polarized antenna with wide beamwidth for GNSS applications," *Progress In Electromagnetics Research C*, Vol. 84, 189–200, 2018.

[6] Akmal, M., A. Alieldin, and A. R. Eldamak, "A printed helical circular polarization antenna for GNSS anti-attacking system," in *2023 International Microwave and Antenna Symposium (IMAS)*, 135–138, Cairo, Egypt, Feb. 2023.

[7] Zhai, J., G. Chen, W. Wang, Y. Liu, L. Wang, and Z. Wang, "A novel low profile circularly polarized GNSS antenna with wide 3 dB axial ratio beamwidth," *Progress In Electromagnetics Research M*, Vol. 111, 199–208, 2022.

[8] Wang, L., Z. Weng, Y.-C. Jiao, W. Zhang, and C. Zhang, "A low-profile broadband circularly polarized microstrip antenna with wide beamwidth," *IEEE Antennas and Wireless Propagation Letters*, Vol. 17, No. 7, 1213–1217, Jul. 2018.

[9] Akmal, M., A. Alieldin, and A. R. Eldamak, "A high-power sandwiched omnidirectional circularly polarized antenna for GNSS systems," *IEEE Access*, Vol. 11, 31 167–31 176, 2023.

[10] Sun, C., H. Zheng, and Y. Liu, "Compact dual-band circularly polarised GNSS antenna," *Electronics Letters*, Vol. 51, No. 20, 1559–1560, Oct. 2015.

[11] Zuo, S.-L., L. Yang, and Z.-Y. Zhang, "Dual-band CP antenna with a dual-ring cavity for enhanced beamwidth," *IEEE Antennas and Wireless Propagation Letters*, Vol. 14, 867–870, 2014.

[12] Zhou, Y., C.-C. Chen, and J. L. Volakis, "Dual band proximity-fed stacked patch antenna for tri-band GPS applications," *IEEE Transactions on Antennas and Propagation*, Vol. 55, No. 1, 220–223, Jan. 2007.

[13] Nikam, A. A. and R. B. Patil, "Integration of LTE and GNSS antenna for multiband performance in vehicular application," *Progress In Electromagnetics Research C*, Vol. 134, 157–169, 2023.

[14] Sun, C., H. Zheng, L. Zhang, and Y. Liu, "A compact frequency-reconfigurable patch antenna for Beidou (COMPASS) navigation system," *IEEE Antennas and Wireless Propagation Letters*, Vol. 13, 967–970, 2014.

[15] Agrawal, N., A. K. Gautam, and K. Rambabu, "Design of single-fed spiral-shaped slotted planar antenna for GPS L2 and L5 applications," *IET Microwaves, Antennas & Propagation*, Vol. 14, No. 15, 1947–1951, Dec. 2020.

[16] Zhu, A., S. Zhu, C. Wan, and A. Zhang, "RPM-loaded compact dual-band circularly polarized antenna for GNSS application," *International Journal of RF and Microwave Computer-Aided Engineering*, Vol. 32, No. 9, e23267, 2022.

[17] Sahana, C., N. M. Devi, and M. Jayakumar, "Multilayer pentagon ring dual-band microstrip antenna for GPS aided GEO augmented navigation receivers," in *2022 IEEE Region 10 Symposium (TENSYMP)*, 1–4, Mumbai, India, Jul. 2022.

[18] Sahana, C. and a. Jayakumar, M. et "Dual-band circularly polarized annular ring patch antenna for GPS-aided GEO-augmented navigation receivers," *IEEE Antennas and Wireless Propagation Letters*, Vol. 21, No. 9, 1737–1741, Sep. 2022.

[19] Sahana, C., M. N. Devi, and M. Jayakumar, "Hexagonal-triangular combinatorial structure based dual-band circularly polarized patch antenna for GAGAN receivers," *IEEE Access*, Vol. 11, 23 205–23 216, 2023.

[20] Choudhary, S. D., A. Srivastava, and M. Kumar, "Design of single-fed dual-polarized dual-band slotted patch antenna for GPS and SDARS applications," *Microwave and Optical Technology Letters*, Vol. 63, No. 1, 353–360, Jan. 2021.

[21] García-Gámez, L., L. Bernard, R. Sauleau, S. Collardey, K. Mahdjoubi, P. Pouliguen, and P. Potier, "Circularly polarized global navigation satellite systems metasurface antennas in sub-wavelength metallic cavities," *International Journal of Microwave and Wireless Technologies*, Vol. 15, No. 8, 1273–1282, Oct. 2023.

[22] Aliqab, K., S. Lavadiya, M. Alsharari, A. Armghan, M. G. Daher, and S. K. Patel, "Design and fabrication of a low-cost, multiband and high gain square tooth-enabled metamaterial superstrate microstrip patch antenna," *Micromachines*, Vol. 14, No. 1, 163, Jan. 2023.

[23] Karmakar, A., "Fractal antennas and arrays: A review and recent developments," *International Journal of Microwave and Wireless Technologies*, Vol. 13, No. 2, 173–197, 2021.

[24] Ellis, M. S., F. B. Effah, A.-R. Ahmed, J. J. Kponyo, J. Nourinia, C. Ghobadi, and B. Mohammadi, "Asymmetric circularly polarized open-slot antenna," *International Journal of RF and Microwave Computer-Aided Engineering*, Vol. 30, No. 5, e22141, 2020.

[25] Chen, Q., H. Zhang, L.-C. Yang, H.-P. Li, T. Zhong, X.-L. Min, and S.-L. Tan, "Novel dual-band asymmetric U-shaped slot antenna for dual-circular polarization," *International Journal of RF and Microwave Computer-Aided Engineering*, Vol. 27, No. 1, e21047, 2017.

[26] Cao, Y. F., S. W. Cheung, and T. I. Yuk, "A multiband slot antenna for GPS/WiMAX/WLAN systems," *IEEE Transactions on Antennas and Propagation*, Vol. 63, No. 3, 952–958, Mar. 2015.

[27] Rabie, M. M., M. S. El-Gendy, A. R. E. Damak, F. Ibrahim, and H. El-Henawy, "A small size wideband m-shaped polygonal slot antenna for X-band satellite applications," *Progress In Electromagnetics Research C*, Vol. 139, 31–43, 2024.

[28] Rabie, M. M., M. S. El-Gendy, A. R. Eldamak, F. Ibrahim, and H. El-Henawy, "A compact wideband circularly polarized fractal slot antenna with rectangular island for X-band satellite applications," *Cogent Engineering*, Vol. 11, No. 1, 2322813, 2024.

[29] Wei, F., X. Liu, X.-Z. Ding, X.-B. Zhao, and P.-Y. Qin, "A balanced filtering antenna array with high gain, steep selectivity, and multi-radiation nulls parallel-fed by differential broadband network," *IEEE Transactions on Antennas and Propagation*, Vol. 71, No. 12, 9926–9931, Dec. 2023.

[30] Dardeer, O. M., H. A. Elsadek, H. M. Elhennawy, and E. A. Abdallah, "Single-fed dual wideband filtenna for 4G/5G mobile applications," *International Journal of RF and Microwave Computer-Aided Engineering*, Vol. 31, No. 5, e22616, 2021.

[31] Sharma, V. and T. Jhajharia, "Square slot antenna for wide circularly polarized bandwidth and axial ratio beamwidth," *Electrical, Control and Communication Engineering*, Vol. 17, No. 1, 1–11, Jun. 2021.

[32] Chen, C.-H. and E. K. N. Yung, "Dual-band circularly-polarized CPW-fed slot antenna with a small frequency ratio and wide bandwidths," *IEEE Transactions on Antennas and Propagation*, Vol. 59, No. 4, 1379–1384, Apr. 2011.

[33] Sze, J.-Y. and S.-P. Pan, "Design of CPW-fed circularly polarized slot antenna with a miniature configuration," *IEEE Antennas and Wireless Propagation Letters*, Vol. 10, 1465–1468, 2011.